Nanoscale

COMMUNICATION

Cite this: *Nanoscale*, 2017, **9**, 4642

Received 20th December 2016,
Accepted 8th March 2017

DOI: 10.1039/c6nr09795b

rsc.li/nanoscale

Direct visualization of carbon nanotube degradation in primary cells by photothermal imaging†

Julie Russier,[a] Laura Oudjedi,[b,c] Martin Piponnier,[b,c] Cyrill Bussy,[d] Maurizio Prato,[e,f,g] Kostas Kostarelos,[d] Brahim Lounis,[b,c] Alberto Bianco*[a] and Laurent Cognet *[b,c]

Assessment of biodegradability of carbon nanotubes (CNTs) is a critically important aspect that needs to be solved before their translation into new biomedical tools. CNT biodegradation has been shown both *in vitro* and *in vivo*, but we are limited by the number of analytical techniques that can be used to follow the entire process. Photothermal imaging (PhI) is an innovative technique that enables the quantitative detection of nanometer-sized absorptive objects. In this study, we demonstrate that PhI allows the observation of the degradation process of functionalized multi-walled carbon nanotubes (MWCNTs) following their internalization by primary glial cells. The absence of interference from the biological matrix components, together with the possibility to combine PhI with other detection techniques (*e.g.* fluorescence, light or electron microscopy) validate the potential of this method to follow the fate and behavior of carbon nanostructures in a biological environment.

The demonstration of the degree of carbon nanotube (CNT) biodegradation is still a challenge in their development for biomedical applications.[1] Although it has been reported that different types of CNTs displayed diverse outcomes when placed in an oxidative environment, there is still a limited number of studies proving their biodegradability in living systems.[2–4] This might be related in part to the very short list of versatile analytical techniques applicable to detect the nanotubes and their fate in cells and organs. Two techniques are commonly employed to follow the progress of CNT degradation: (i) transmission electron microscopy (TEM), and (ii) Raman spectroscopy or imaging.[1,5]

TEM enables the visualization of the CNT physical structure evolution and measurement of the changes in the CNT length and diameter during the incubation with oxidative enzymes.[2,3,6] However, TEM has certain limitations particularly when performed directly in biological matrices such as cells and tissues, where the contrast of organic components (*i.e.* carbon based) might hamper a clear identification of degrading carbon nanotubes.

Raman spectroscopy is also a powerful tool to evaluate the integrity of CNT crystalline structures that can then be extrapolated to their physical structures.[7] In fact, CNTs show two main characteristic bands in the Raman spectrum, corresponding to G (~1590 cm^{-1}) and D (~1350 cm^{-1}) bands, describing the graphitic structure of CNT sidewalls and the defect sites, respectively.[8] It is easy to recognize and follow the evolution of these two signals along the degradation process. Nevertheless, Raman spectroscopy also presents some limitations. Even in the absence of degradation, it is difficult to analyze some MWCNTs that show a strong D band due to the presence of a high amount of defects on their sidewalls. Secondly, Raman spectroscopy gives information only about the sidewall structure of CNTs and does not provide any data about their length, which has been proven to be shortened by oxidative enzymes during their biodegradation.[2,3,6] Finally, the definition of the Raman signal and therefore the analysis of Raman spectra are highly affected by the auto-fluorescence of biological specimens and the selection of the substrate used to collect the Raman signal. Although the combination of TEM and Raman spectroscopy helps in an overall analysis of the biodegradation process,[5,6,9,10] the use of alternative techniques with lower interference from the biological matrix components could be highly advantageous to study *in situ* the CNT degradation in complex biological systems.

[a]*University of Strasbourg, CNRS, Immunopathology and Therapeutic Chemistry, UPR 3572, 67000 Strasbourg, France. E-mail: a.bianco@ibmc-cnrs.unistra.fr*
[b]*University of Bordeaux, LP2N, F-33405 Talence, France. E-mail: laurent.cognet@u-bordeaux.fr*
[c]*Institut d'Optique & CNRS, LP2N, F-33405 Talence, France*
[d]*Nanomedicine Laboratory, Faculty of Biology, Medicine and Health and National Graphene Institute, University of Manchester, AV Hill Building, Manchester M13 9PT, UK*
[e]*Dipartimento di Scienze Chimiche e Farmaceutiche, Università di Trieste, Trieste 34127, Italy*
[f]*Carbon Nanobiotechnology Laboratory, CIC biomaGUNE, Paseo de Miramón 182, 20009 Donostia-San Sebastian, Spain*
[g]*Basque Fdn Sci, Ikerbasque, Bilbao 48013, Spain*

†Electronic supplementary information (ESI) available: Experimental section including materials and methods. See DOI: 10.1039/c6nr09795b

In this context, photothermal imaging (PhI) could be a good candidate, as it enables the efficient detection of nanometer-size objects solely based on their absorption, and does not have the burden of biological matrix component interference, observed with TEM or Raman based *in situ* degradation evaluations. The extreme sensitivity of the PhI method and the stability of the signals have already opened the way to numerous applications in spectroscopy, analytical chemistry and bioimaging.[11,12] Like Raman spectroscopy, PhI is an all-optical method, and it is based on the detection of refractive index variations that are induced by the photothermal effect in the local environment of an absorbing nanoparticle.[13,14] A few variants of PhI exist,[13,15,16] and photothermal heterodyne imaging, which is the most sensitive scheme,[13,17] allows the detection of several types of nanoobjects at a single particle level. These include gold nanoparticles, even within a cell matrix and for membrane receptor dynamics studies in live cells,[18,19] molecules, quantum dots or single walled carbon nanotubes.[19–25] Interestingly, PhI signal intensities can be correlated with the dimension[26] and concentration[27] of the nanoparticles under investigation, while quantitative optical imaging of individual nanotubes down to ~10 nm in length was possible.[28] In addition, PhI is totally unaffected by non-absorbing scatterers, even when large objects with strong refractive index contrast are present within the surroundings of the imaged nanoparticles, as it is often the case in biological samples. In view of these advantageous characteristics we decided to explore the potential of this technique for the direct visualization of functionalized carbon nanotube degradation inside microglia, the resident macrophages of the central nervous system, and their evolution overtime. Here we based our demonstration on these primary microglial cells owing to previous experience with this model (same primary cells and same functionalized CNTs, see below) using TEM or Raman to assess degradation, hence providing a direct comparison with previously reported data.[29]

We thus used MWCNTs functionalized by the 1,3-dipolar cycloaddition reaction, leading to cationic nanotubes (MWCNT-NH_3^+) (Fig. 1).[30,31]

This type of nanotube has been extensively used for different applications including therapy and imaging.[32–34] In particular, they have been explored as carriers of small interference RNA for gene silencing.[32,33] Their biodistribution and biodegradation have also been thoroughly assessed.[5,35] In this context, we recently studied the kinetics of degradation of MWCNTs with different types of functionalizations into long-term cultures of microglia using Raman spectroscopy.[29] Functionalization including the 1,3-dipolar cycloaddition reaction was able to promote a continuous and progressive intracellular degradation of these different nanotubes over three months.[29]

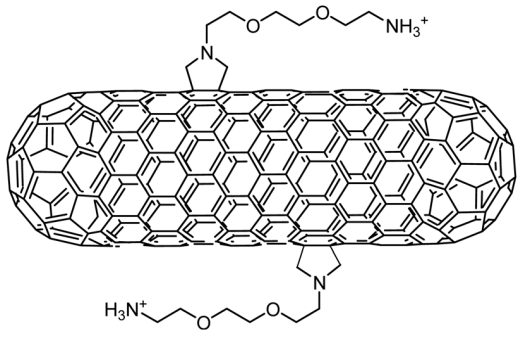

Fig. 1 Molecular structure of functionalized multi-walled carbon nanotubes (MWCNT-NH_3^+).

Semi-thin or ultra-thin sections of about 500 nm and 70 nm, respectively, are often used for TEM analysis of biological specimens embedded in resin. We thus decided to determine whether we could observe nanotubes and evaluate the progression of their degradation in microglial cells by PhI using semi-thin sections. MWCNT-NH_3^+ were first incubated with primary microglial cells for 24 h. The cells were subsequently maintained in culture for different periods of times (1, 7 and 14 days) at the end of which the CNT loaded cells were fixed, embedded in resin and sectioned, before imaging by PhI (experimental setup in Fig. S1†). Fig. 2 shows photoluminescence (GFP channel) and PhI images of representative regions of microglial cells that were incubated with MWCNT-NH_3^+ and then fixed after 1, 7 or 14 days of culture. For each of the three time points, PhI signals reveal the unambiguous presence of intracellular MWCNTs in comparison to the cells that were not exposed to MWCNTs (Fig. S2†). Moreover, while MWCNT-NH_3^+ were present in large aggregates inside cells at day 1 (Fig. 2), they appeared more dispersed and more individualized after 14 days, suggesting their partial intracellular degradation or clearance (Fig. 2).

To further quantify these observations, we performed a systematic analysis of PhI signals by measuring the signal surface areas and the intensities detected in the cells at different time points (Fig. 3). After image segmentation, the cumulative histograms of the signal areas were plotted in Fig. 3A, normalized to the point-spread function of the microscope (~290 nm, see ESI†). In each segmented area, signal intensities defined as integrated signals normalized by the surface areas were also measured and are displayed in Fig. 3B.

The evolution of both signal areas and intensities from day 1 to day 14 indicates that nanotubes become sparser and less absorptive (Fig. 3A and B, respectively), consolidating the idea of their intracellular degradation as suggested by observations in Fig. 2 and as previously reported for the same nanotubes using Raman spectroscopy.[29] Interestingly, at day 7 and day 14, histograms of signal areas (Fig. 3A) are almost identical, while signal intensities (Fig. 3B) are smaller at day 14 than at day 7. This led us to speculate that the intracellular nanotube degradation may start by a combined process of de-agglomeration and shortening of the MWCNTs from day 1 to day 7 (*i.e.* combined area and intensity reduction) followed by thinning of the nanotube diameters *via* degradation of their outer walls beyond day 7 (*i.e.* only intensity reduction).

Altogether, these findings (Fig. 2 and 3) suggest the intracellular degradation or removal of MWCNTs, thus confirming

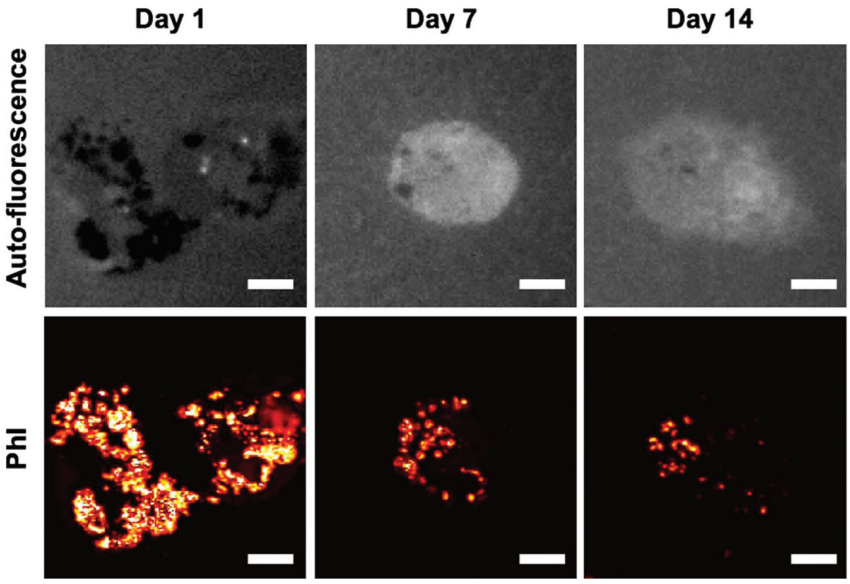

Fig. 2 Photoluminescence (top row) and PhI images (bottom row) of 500 nm semi-thin sections of resin embedded microglial cells incubated with MWCNT-NH_3^+ at 10 μg ml^{-1} and then cultured for 1, 7 and 14 days. Scale bar: 5 μm.

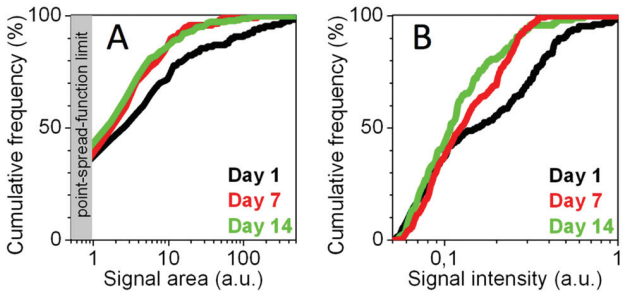

Fig. 3 Analysis of the PhI signal area (A) and intensity (B) related to MWCNT-NH_3^+ (10 μg ml^{-1}) in microglial cells after 1 to 14 days. The graphs represent the cumulative distributions, normalized to 100, of PhI signal areas and intensities detected in cells (131, 119 and 334 analyzed areas in 9, 7, and 14 cells for 1, 7 and 14 days, respectively).

previous evidence of intracellular degradation of these same nanotubes stereotactically injected into mouse brain or cultured in isolated primary microglia (using TEM, Raman spectroscopy, or both).[5,29] However, our present investigations revealed that for characterizing the evolution of the CNT content in biological samples, PhI presents key advantages with respect to TEM and Raman spectroscopy, which are currently the two main established methods for such characterization. In particular, and in contrast to both TEM and Raman spectroscopy/imaging, PhI has the advantage of having no interference from biological matrix components that could hamper the CNT degradation analysis (*i.e.* carbon in carbon-based matrix and auto-fluorescence, for TEM and Raman, respectively). In addition, PhI allows exploiting the standard preparation procedures of biological samples used for other microscopic analysis techniques, such as resin embedding for TEM or paraffin embedding for histology. The possibility to prepare one biological sample for multiple observations such as PhI and TEM or PhI and histology allows the development of correlative microscopy strategies. This could be of high interest to further study the intracellular trafficking and fate of CNTs in combination to evaluate their biological impact.

In summary, this study provides evidence that PhI can be used alongside TEM and Raman spectroscopy as a simple characterization technique for both *in situ* visualization and evaluation of MWCNT degradation in cells as a function of time. Moreover, PhI does not share the limitations of TEM and Raman spectroscopy in regard to *in situ* CNT degradation evaluation. Finally, this technique can easily be expanded to any biological samples as specimen preparation requirements are similar to other analytical microscopy techniques (TEM, histology).

Acknowledgements

This work was supported by the Centre National de la Recherche Scientifique (CNRS), DGA, the International Center for Frontier Research in Chemistry (icFRC), the France-BioImaging national infrastructure (ANR-10-INBS-04-01), IdEx Bordeaux (ANR-10-IDEX-03-02), the Agence Nationale de la Recherche (ANR) (ANR-14-OHRI-0001-01 & ANR-15-CE16-0004-03) and by ANR through the LabEx project Chemistry of Complex Systems (ANR-10-LABX-0026_CSC). CB would like to acknowledge a fellowship from the European Commission, under the FP-7 people Marie Curie Actions (Career Development Intra-European Fellowship, FP7- PIEF-GA-2010-276051, project NANONEUROHOP). M. P. acknowledges financial support from the AXA Chair program.

References

1 A. Bianco, K. Kostarelos and M. Prato, *Chem. Commun.*, 2011, **47**, 10182.
2 G. P. Kotchey, S. A. Hasan, A. A. Kapralov, S. H. Ha, K. Kim, A. A. Shvedova, V. E. Kagan and A. Star, *Acc. Chem. Res.*, 2012, **45**, 1770–1781.
3 G. P. Kotchey, Y. Zhao, V. E. Kagan and A. Star, *Adv. Drug Delivery Rev.*, 2013, **65**, 1921–1932.
4 D. Elgrabli, W. Dachraoui, C. Ménard-Moyon, X. J. Liu, D. Bégin, S. Bégin-Colin, A. Bianco, F. Gazeau and D. Alloyeau, *ACS Nano*, 2015, **9**, 10113–10124.
5 A. Nunes, C. Bussy, L. Gherardini, M. Meneghetti, M. A. Herrero, A. Bianco, M. Prato, T. Pizzorusso, K. T. Al-Jamal and K. Kostarelos, *Nanomedicine*, 2012, **7**, 1485–1494.
6 J. Russier, C. Ménard-Moyon, E. Venturelli, E. Gravel, G. Marcolongo, M. Meneghetti, E. Doris and A. Bianco, *Nanoscale*, 2011, **3**, 893–896.
7 B. L. Allen, P. D. Kichambare, P. Gou, I. I. Vlasova, A. A. Kapralov, N. Konduru, V. E. Kagan and A. Star, *Nano Lett.*, 2008, **8**, 3899–3903.
8 J. Bartelmess, S. J. Quinn and S. Giordani, *Chem. Soc. Rev.*, 2015, **44**, 4672–4698.
9 A. R. Sureshbabu, R. Kurapati, J. Russier, C. Ménard-Moyon, I. Bartolini, M. Meneghetti, K. Kostarelos and A. Bianco, *Biomaterials*, 2015, **72**, 20–28.
10 Y. Zhao, B. L. Allen and A. Star, *J. Phys. Chem. A*, 2011, **115**, 9536–9544.
11 L. Cognet, S. Berciaud, D. Lasne and B. Lounis, *Anal. Chem.*, 2008, **80**, 2288–2294.
12 P. Vermeulen, L. Cognet and B. Lounis, *J. Microsc.*, 2014, **254**, 115–121.
13 S. Berciaud, L. Cognet, G. A. Blab and B. Lounis, *Phys. Rev. Lett.*, 2004, **93**, 257402.
14 M. Selmke, M. Braun and F. Cichos, *ACS Nano*, 2012, **6**, 2741–2749.
15 D. Boyer, P. Tamarat, A. Maali, B. Lounis and M. Orrit, *Science*, 2002, **297**, 1160–1163.
16 V. P. Zharov, V. Galitovsky and M. Viegas, *Appl. Phys. Lett.*, 2003, **83**, 4897.
17 A. Gaiduk, M. Yorulmaz, P. V. Ruijgrok and M. Orrit, *Science*, 2010, **330**, 353–356.
18 D. Lasne, G. A. Blab, S. Berciaud, M. Heine, L. Groc, D. Choquet, L. Cognet and B. Lounis, *Biophys. J.*, 2006, **91**, 4598–4604.
19 C. Leduc, S. Si, J. Gautier, M. Soto-Ribeiro, B. Wehrle-Haller, A. Gautreau, G. Giannone, L. Cognet and B. Lounis, *Nano Lett.*, 2013, **13**, 1489.
20 M. A. van Dijk, M. Lippitz and M. Orrit, *Acc. Chem. Res.*, 2005, **38**, 594–601.
21 S. Berciaud, L. Cognet and B. Lounis, *Nano Lett.*, 2005, **5**, 2160–2163.
22 S. Berciaud, L. Cognet, P. Poulin, R. B. Weisman and B. Lounis, *Nano Lett.*, 2007, **7**, 1203–1207.
23 C. Leduc, J.-M. Jung, R. R. Carney, F. Stellacci and B. Lounis, *ACS Nano*, 2011, **5**, 2587–2592.
24 P. Zijlstra, P. M. R. Paulo and M. Orrit, *Nat. Nanotechnol.*, 2012, **7**, 379–382.
25 J. Olson, S. Dominguez-Medina, A. Hoggard, L.-Y. Wang, W.-S. Chang and S. Link, *Chem. Soc. Rev.*, 2015, **44**, 40–57.
26 S. Berciaud, D. Lasne, G. A. Blab, L. Cognet and B. Lounis, *Phys. Rev. B: Condens. Matter*, 2006, **73**, 045424.
27 L. Cognet, C. Tardin, D. Boyer, D. Choquet, P. Tamarat and B. Lounis, *Proc. Natl. Acad. Sci. U. S. A.*, 2003, **100**, 11350–11355.
28 Z. Gao, L. Oudjedi, R. Faes, F. Moroté, C. Jaillet, P. Poulin, B. Lounis and L. Cognet, *Sci. Rep.*, 2015, **5**, 17093.
29 C. Bussy, C. Hadad, M. Prato, A. Bianco and K. Kostarelos, *Nanoscale*, 2016, **8**, 590–601.
30 H. Ali-Boucetta, A. Nunes, R. Sainz, M. A. Herrero, B. Tian, M. Prato, A. Bianco and K. Kostarelos, *Angew. Chem., Int. Ed.*, 2013, **52**, 2274–2278.
31 V. Georgakilas, N. Tagmatarchis, D. Pantarotto, A. Bianco, J.-P. Briand and M. Prato, *Chem. Commun.*, 2002, 3050–3051.
32 K. T. Al-Jamal, L. Gherardini, G. Bardi, A. Nunes, C. Guo, C. Bussy, M. A. Herrero, A. Bianco, M. Prato, K. Kostarelos and T. Pizzorusso, *Proc. Natl. Acad. Sci. U. S. A.*, 2011, **108**, 10952–10957.
33 J. E. Podesta, K. T. Al-Jamal, M. A. Herrero, B. Tian, H. Ali-Boucetta, V. Hegde, A. Bianco, M. Prato and K. Kostarelos, *Small*, 2009, **5**, 1176.
34 L. G. Delogu, G. Vidili, E. Venturelli, C. Menard-Moyon, M. A. Zoroddu, G. Pilo, P. Nicolussi, C. Ligios, D. Bedognetti, F. Sgarrella, R. Manetti and A. Bianco, *Proc. Natl. Acad. Sci. U. S. A.*, 2012, **109**, 16612–16617.
35 K. T. Al-Jamal, A. Nunes, L. Methven, H. Ali-Boucetta, S. Li, F. M. Toma, M. A. Herrero, W. T. Al-Jamal, H. M. M. ten Eikelder, J. Foster, S. Mather, M. Prato, A. Bianco and K. Kostarelos, *Angew. Chem., Int. Ed.*, 2012, **51**, 6389–6393.